2017 IEEE/RSJ International Conference on Intelligent Robots and Systems (IROS)
September 24–28, 2017, Vancouver, BC, Canada

Design and Development of a Mobile Crawling Robot with Novel Halbach Array Based Magnetic Wheels

W.A.V.Stepson, A.D.I.M. Amarasinghe, P.N.R. Fernando, Y.W.R. Amarasinghe
Department of Mechanical Engineering,
University of Moratuwa, Sri Lanka

***Abstract*— higher efficiency and the safety of hull inspection can be achieved by replacing the conventional methods with modern crawling robots. This paper consists of detailed study of the design and development of a crawling robot with a novel permanent magnetic wheel based on Halbach magnetic array. The magnetic array and the wheel assembly were designed based on the magnetic simulation results. Maintaining the adequate adhesion force as well as the friction force of the wheels were considered in designing the wheels. The crawling robot is equipped with a steering system based on Ackermann steering method hence the steering angles are controlled by an algorithm and actuated using servo motors. The driving system of the robot is equipped with four geared stepper motors and they are controlled separately by the algorithm according to the inputs of the controller. The control architecture and the components used for the robot control system are explained. The operator can remotely control the robot and inspect the hull surface via the camera feed available in the HMI (Human Machine Interface) of the robot. The prototype of the crawling robot was tested in a similar environment and the test results are included in the paper.**

I. INTRODUCTION

The dry-dock ship hull inspection is significant in identifying the defects of the ship hull plates before repairing or replacing them. Corrosion, wear, tear, cracks and indentations of the hull surface are mainly inspected within the inspection processes. An inspector reaches the hull surface and inspects the hull plates manually using inspection instruments in conventional methods and those methods incorporate lot of drawbacks. Reaching the hull plates using cherry pickers, staging or scaffoldings, ladder and cranes are very expensive and time consuming. They require several persons for the task and there is a certain degree of danger.

Several robots have already been developed for various climbing applications. compared to the current conventional methods, ship hull inspection with robots is more efficient, safe and cost effective.

The locomotion method, which provides the motion on the crawling surface and the adhesion method, which keeps the robot in contact with the crawling surface are the main design concerns of crawling robots. Tracked [1][2], legged [3][4], and wheeled locomotion methods are commonly used locomotion methods in crawling robots. Pneumatic suction [9][10], dry adhesion [11], propeller adhesion [12] and magnetic adhesion [5-8] are widely used adhesion methods in crawling robots.

The crawling robot presented in this paper consists of four specially designed compact magnetic wheels adapting Halbach magnetic array.

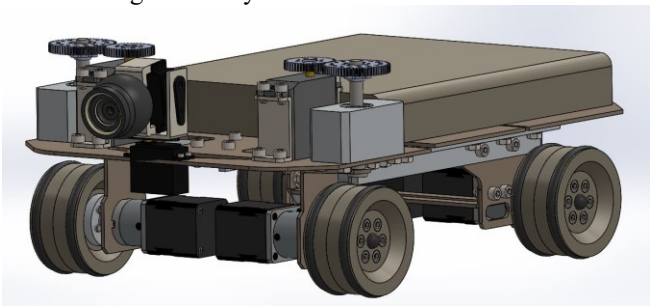

Figure 1.3D model of the crawling robot

II. WORKING ENVIRONMENT OF THE ROBOT

The crawling robot presented in this paper is the prototype of a crawling robot for ship hull inspection at the dry dock. The robot was designed to operate on ferromagnetic ship hulls. The hull surfaces of the ships which are taken for the inspection generally have irregularities due to rugged operation in corrosive environments. These ship hulls may consist of convex and concave surfaces with large curvatures and flat surfaces. The robot should be able to climb on vertical and inclined surfaces. The welding seams along the hull surface are the obstacles for the robot. Considering the above facts remotely controlled crawling robot consisting four magnetic wheels was designed for ship hull inspection task.

III. STATE OF THE ART

Modern climbing robots are developed using various combinations of locomotion and adhesion methods according to their application. Wheeled locomotion and magnetic adhesion are mainly considered in this section.

A. Wheeled Locomotion

Wheeled locomotion is commonly used in climbing robots due to simple design, easy control and high speed. The magnet wheel mechanism used in [6] is designed especially for metal pipe inspection. It can go through obstacles, gaps and cavities inside pipes. In some cases, adhesion method is separated from the wheel locomotion and attached to the structure of the robot. In [5] robot, four permanent magnets are attached to the surface while the robot is driven by individually controlled four wheels. Separate locomotion is easier to control due to the lack of magnetic effect on wheels. There are robots with adhesion methods embedded into the wheels [7][8]. The contact area of the wheel affects

the magnetic flux and by changing the shape of the contact area, the magnetic flux can be manipulated as desired [7].
Wheels of the climbing robot have to deliver sufficient amount of friction to drive on the surface. The climbing robot in [7] has permanent magnet wheels which are covered with rubber tires to increase the friction between the surface and the wheels.
Magnet embedded wheels are difficult to maneuver. Therefore, a multi-segmented chassis is used in climbing robot in [8]. Some robots are made with two magnet wheels and a single or multiple normal wheels for steering [13].

B. *Magnetic Adhesion*

Magnetic adhesion can be used on ferromagnetic surfaces. Magnets can exert large amount of adhesion forces compared to other methods so that the payload capacity of the robots can be increased. Magnetic adhesion can be achieved using permanent magnets, electromagnets and electro-permanent magnets. Permanent magnets are reliable for climbing robots as no external power source is needed. Permanent magnets are highly brittle and they can be easily corroded upon direct expose to the environment. Therefore, permanent magnets need proper protection and avoiding direct contact with the working surface is recommended [7].
Magnets can be embedded to wheels [7][8][13] and tracks or attached separately in the chassis of the robot [10]. In both cases, the actual distance from the magnet to the ferromagnetic surface should be small to maximize the magnetic effect. To avoid losses in magnetic flux, the materials used proximity to the magnets have to be non-magnetic [7][8].

IV. HALBACH ARRAY

High-torque motors, Maglevs and MRI scanners are equipped with Halbach magnetic arrays to increase the generated flux in desired directions. Halbach magnetic array can augment the magnetic flux towards a single direction by cancelling the magnetic flux of the other directions. The one-sided flux effect of Halbach array is resulted by the cancellation of magnetic components of the adjacent magnets in the array. This phenomenon can be used for developing a magnet wheel with a very large magnetic force. Adapting the Halbach magnetic array for a wheel design requires augmentation of magnetic flux in radially outwards direction. A circular array is used for the wheel.

V. CALCULATION OF REQUIRED MAGNETIC FORCE

The weight of the proposed robot was determined to be 12 kg and a payload of 8 kg was expected. Therefore, the total weight (*m)* value was taken as 20 kg for calculations.
Considering these facts, the formula for required magnetic adhesion force (R_M) of a wheel was derived incorporating, inclination of the working plane to the horizontal (α), coefficient of friction between the wheel and the ferromagnetic surface (μ_s) and total mass of the robot (m).

$$R_M = 49.05[\sin(\alpha)/\mu_s - \cos(\alpha)] \quad (1)$$

The distribution of R_m was studied varying α and μ_s, using MATLAB software to identify the maximum required magnetic adhesion force of a magnetic wheel (R_{max}). The lowest margin for μ_s value between Aluminium and Mild Steel was chosen as 0.5 as the μ_s value is typically more than 0.6 and special arrangements of the wheel design to increase the μ_s value are discussed in the following sections. The respective R_{max} value of 109.7 N for 0.5 of μ_s at $\alpha = 116^o$ was chosen to proceed with the design.

VI. MAGNGETIC WHEEL DESIGN

A circular magnetic array with 16 segment magnets was designed to integrate into the wheel assembly. This magnetic array consists of three types of segment magnet units which are magnetized differently. They are diametric outer N pole, diametric inner N pole and magnetized through width segment magnet units as shown in "Fig. 3".

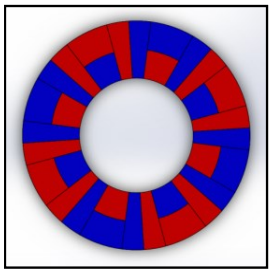

Figure 2. Magnet Array Assembly

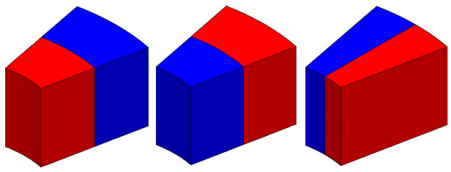

Outer N Pole Outer S Pole Through Width

Figure 3. Three types of magnets

Neodymium N52 rare earth magnets were used for the magnet array due to high magnetic flux density. The magnetic simulations of the magnetic array design were conducted with COMSOL multi-physics software. The array was simulated varying the outer diameter, inner diameter and thickness of the magnetic array. Adhesion force between the outer circular surface of the magnetic array and ferromagnetic plate with 10mm thickness was studied and the results were graphed. We proceeded with 80 mm of outer diameter, 40 mm of inner diameter and 15 mm of thickness values for the array design. According to the simulation results, 247.9N of adhesion force can be achieved between the outer circular surface and the ferromagnetic plate with 10mm of thickness.

During the operations, the magnets has to be protected from direct touch with the working surface to prevent breaking. And the magnets should be properly covered to prevent corrosion. Introducing an outer casing for the magnet array cause the reduction of magnetic adhesion force between the wheel and the crawling surface. The permeability of the casing material weakens the magnetic adhesion force of the

wheel. Aluminium has very low relative permeability value of 1.0000037. Aluminium 1060 was chosen as the casing material for the wheel design considering both magnetic and physical properties of the materials.

The outer casing thickness makes a gap between the ferromagnetic crawling surface and the magnetic array and the magnetic adhesion force is weakened. A simulation was conducted with COMSOL multi-physics software to study the behavior of the magnetic adhesion force with the thickness of the Aluminium outer casing. The thickness was varied from 1mm to 5mm. The adhesion force is decreased exponentially with the thickness of the outer casing as it creates a gap between the magnet array and the ferromagnetic crawling surface. Based on simulation results 2mm of thickness was chosen for the Aluminium outer casing and an overall 156.7N of magnetic adhesion force could be generated between the wheel and the ferromagnetic surface with 10mm thickness.

Special arrangement of rubber friction bands was designed to be accommodated at the outer circular surface with the intension to increase the friction force between the wheel and the crawling surface. Generally dynamic friction coefficient between Aluminium and Steel is 0.61 and static coefficient value around 1.0 can be achieved by introducing the rubber friction bands to the wheels.
The complete wheel assembly consists of these components. (1) M5 thrust screw, (2) mounting flange, (3) friction band, (4) inner wheel casing, (5) rubber pad, (6) magnet array, (7) outer wheel casing, (8) rubber cap, (9) M6x40 Allen bolts.

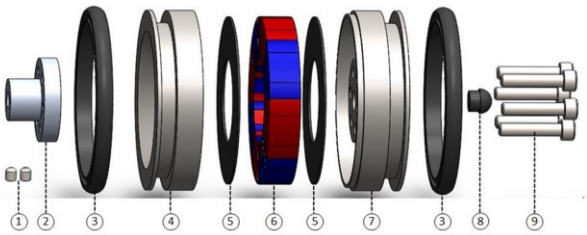

Figure 4. Exploded view of the wheel

VII. DRIVE SYSTEM

Four separate stepper motors are used to drive the four magnetic wheels of the mobile robot. If the two-wheel drive method is used, the driving wheels have to overcome the resistant friction forces against the motion exerted by the remaining driven wheels and extra torques are needed for the motors which drive the driving wheels. This requirement of extra motor torques can be avoided by using four-wheel drive method.Four magnetic wheels with 80mm outer diameter and 40mm thickness are connected to four separate NEMA 17 Bi-polar 14:1 Geared Steppers and they are driven separately with four TB6600 stepper drives. 24V voltage supply is provided to the steppers through the motor drivers. Rear two wheels are mounted to the fixed brackets of the main structure with the motors. Front wheels are able to turn by the servo motors according to the inputs from the console.

VIII. STEERING SYSTEM

Although the steering system of the mobile robot is based on Ackermann principle the space between the front wheels is packed with the motors and it is difficult to accommodate track-rod and steering-arms due to lack of space. Considering this situation, the steering system of the crawling robot was designed eliminating all the mechanical linkages such as track-rod and steering-arms which comes in Ackermann mechanism and two separate servo motors were engaged to control the steering angles of the two front wheels. The coordination of the two steering angles is controlled by the algorithm. The algorithm for the steering system was developed based on the following calculation.

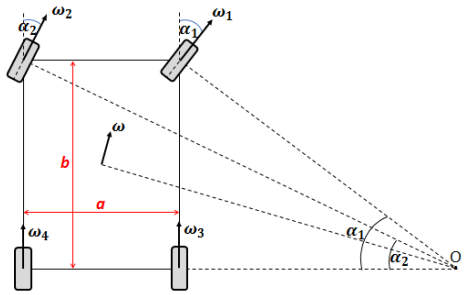

Figure 5. Steering angles and wheel speeds

Considering steering angle of front right wheel (α_1), steering angle of front left wheel (α_2), length of axle (a), distant between front and rear axles (b), according to the the Ackermann equation,

Case 1: Clockwise turn of the robot

$$Cot(\alpha_1)-Cot(\alpha_2) = a/b \qquad (2)$$

Case 2: Anti-clockwise turn of the robot

$$Cot(\alpha_2)-Cot(\alpha_1) = a/b \qquad (3)$$

The front right wheel is controlled by the joystick and the front left wheel is turned according to the calculated steering angle by the algorithm. SR 811 Servo Motors has 33kgcm of torque and the torque is transferred to the steering mechanism of the wheels with a gear mechanism with a gear ratio of 1.3. The gear mechanism helps to increase the torque provided by the servo motor by 1.3 times.

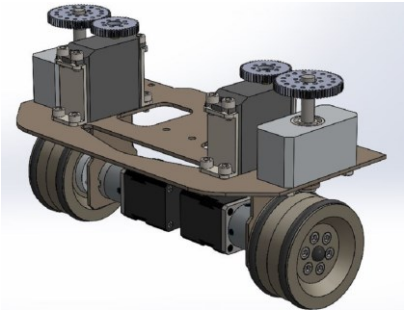

Figure 6. Steering Mechanism

The mechanical limit of the SR 811 is 180 degrees. Approximately 135 degree range can be achieved after the gear mechanism. When the robot is taking a bend, the rotation speeds of the four wheels also should be different to each other as the four wheels of the robot trace in four circles with different radii. The synchronization of the speeds of four wheels should also be controlled for coordinated turn without slipping. The algorithm for rotation speeds of the wheels was developed based on the calculations incorporating steering angles. Considering the point O as where the projected centerlines of the wheels meet and Rotational speed of imaginary center-point wheel *(w),* Rotational speed of front right wheel*(w_1),* Rotational speed of front left wheel*(w_2),* Rotational speed of rear right wheel*(w_3)* , Rotational speed of rear left wheel*(w_4)*

Case 1: Clockwise rotation of the robot

$$w_1=2bw/Sqrt[3b^2Cos^2(\alpha_1)+b^2+a^2Sin^2(\alpha_1)+2abSin(2\alpha_1)] \quad (4)$$

$$w_2=2bwSin(\alpha_1)/\{Sqrt[3b^2Cos^2(\alpha_1)+b^2+a^2Sin^2(\alpha_1)+2abSin(2\alpha_1).Sin(\alpha_2)]\} \quad (5)$$

$$w_3=2bwCos(\alpha_1)/Sqrt[3b^2Cos^2(\alpha_1)+b^2+a^2Sin^2(\alpha_1)+2abSin(2\alpha_1) \quad (6)$$

$$w_4=2bwCot(\alpha_2)Sin(\alpha_1)/\{Sqrt[3b^2Cos^2(\alpha_1)+b^2+a^2Sin^2(\alpha_1)+2abSin(2\alpha_1)]\} \quad (7)$$

Case 2: Anti-Clockwise rotation of the robot

$$w_1=2bwSin(\alpha_1)Sin(\alpha_2)/Sqrt(3b^2Cos^2(\alpha_1)+b^2+a^2Sin^2(\alpha_1)+2abSin(2\alpha_1)) \quad (8)$$

$$w_2=2bw/Sqrt[3b^2Cos^2(\alpha_1)+b^2+a^2Sin^2(\alpha_1)+2abSin(2\alpha_1)] \quad (9)$$

$$w_3=2bwCot(\alpha_1)Sin(\alpha_2)/Sqrt[3b^2Cos^2(\alpha_1)+b^2+a^2Sin^2(\alpha_1)+2abSin(2\alpha_1)] \quad (10)$$

$$w_4=2bwCos(\alpha_2)/Sqrt[3b^2Cos^2(\alpha_1)+b^2+a^2Sin^2(\alpha_1)+2abSin(2\alpha_1)] \quad (11)$$

The value of w can be controlled by the operator and the rotational speeds w_1, w_2, w_3 , w_4 values are calculated by the algorithm and fed to the driving stepper motor of the particular wheel. According to the robot design *a* and *b* values are respectively 300mm and 450mm and the minimum turning radius is 640.8mm.

IX. Control Architecture and HMI

The control system of the robot consists of two main units. They are the console and the mobile platform. The console and the display acts as the Human Machine Interface (HMI) of the robot and it takes input parameters from the console and the camera feed of the robot can be seen on the display.

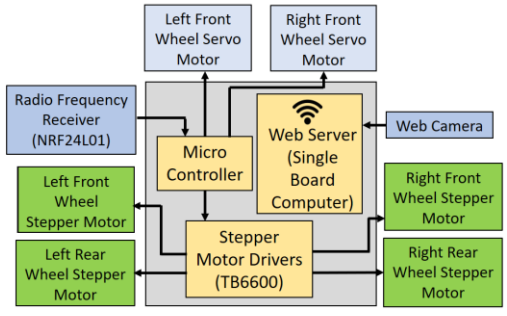

Figure 7. Control diagram of mobile platform

The inputs taken from the console are steering angle, required speed of the robot, Run/Stop input and Forward/ Reverse direction input. The algorithm for steering angle calculation and the algorithm to calculate the rotational speeds of the four wheels are integrated to the Arduino in the console to reduce the processing load of the controller in mobile platform.

The micro controller in the mobile platform is used for driving stepper motors and two steering servo motors. NRF transmitter-receiver modules are used to pass the input parameters to the Arduino in mobile platform. The mobile platform is equipped with Arduino Mega 2560 micro controller board and a Raspberry Pi3-Model B single board computer. The four stepper motors are driven using TB6600 stepper drivers. The camera unit connected to Raspberry Pi single board computer acquires the camera input and stream via a local wireless network.

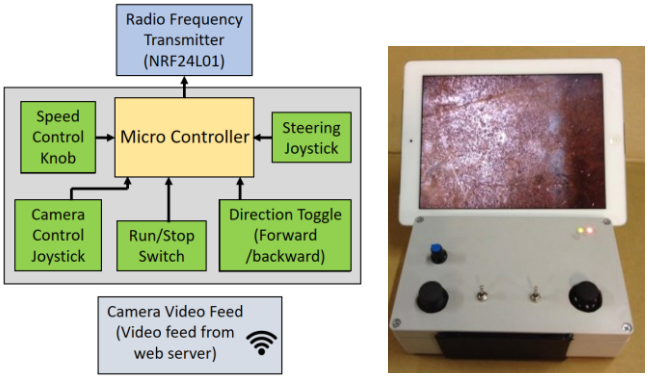

Figure 9. Control diagram of the console (left), HMI (right)

The console is equipped with two, two-axis analog joysticks, analog potentiometer and two switches to control the input parameters for the robot. An Arduino UNO is used in the console to read the input signals from the input devices. The Ackermann algorithms to calculate the particular steering angles of the left and right front wheels and the rotation speeds of the four wheels are programmed in the Arduino UNO. The calculated parameter values and the signals from the input devices are communicated from the console to the robot control system with a NRF module via radio frequency.

An iPad is used as the output display of the HMI. The camera feed taken from the camera mounted on the robot is streamed by the Raspberry Pi3 model-b used in the robot and the video stream is accessed by the iPad through a local network.

X. Results and Validation

A. Fabrication

Materials used for the structure of the robot are Aluminium 1060 and Mild Steel. The structural components are made of Mild Steel and the remaining components are made with Aluminium 1060. Precise dimensions of the structure were achieved by CNC machining with tolerances of 0.05 mm.

Figure 10. Wheel assembly

B. *Field Testing*

As the first field testing, the prototype of our crawling robot was tested at the University of Moratuwa on a ferromagnetic structure with a rusted surface and the thickness of the plate was 6mm.

The prototype was kept on the surface and the ability to stay in contact with the ferromagnetic surface was checked. The robot was kept on the vertical plane (a) facing right side, (b) facing diagonally and (c) facing upwards. The crawling robot remained steady on the ferromagnetic surface without slipping at above all configurations. At (b) and (c) configurations the robot tended to freely roll when the power was 'off' status due to absence of the holding torques of the driving stepper motors. The robot stayed without slipping and rolling at all the (a), (b) and (c) configurations when the power was 'On'.

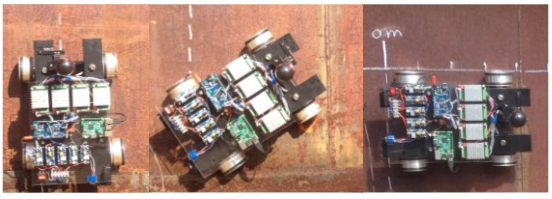

(a) (b) (c)

Figure 11. Static holding test

Next the locomotion ability of the robot was tested on the ferromagnetic surface. The robot was driven on the vertical plane on a path parallel to the horizontal and the robot completed the 2m distance in 10 seconds.

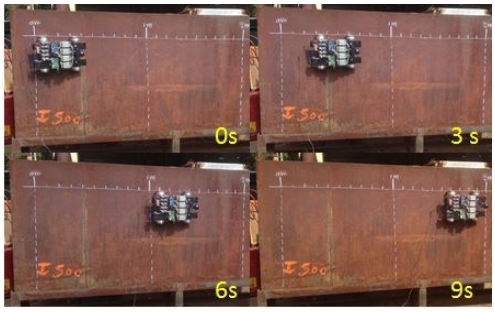

Figure 12. Dynamic test 1

Next the robot was driven on the vertical ferromagnetic structure in vertically up direction. The robot could travel 1m distance in 6 seconds' time period.

Figure 13. Dynamic test 2

Next the robot was driven on the vertical ferromagnetic surface diagonally upward path which is inclined to the horizontal. The robot could travel approximately 1.4m distance in 6 seconds.

Figure 14. Dynamic test 3

The functionalities of the console, steering joystick controls, run/stop function, direction changing function, camera mount control function using the joystick were tested one by one and the prototype robot responded according to the desired results.

The wireless communication and the video streaming were tested increasing the distance between the prototype and the HMI. The prototype robot was able to operate with complete functionality until 40m range between the robot and the HMI.

The completely fabricated mobile robot was tested on an actual ship hull at the dry-dock of Colombo Dockyard PLC as the second field testing and the main purposes of this testing was to test the behavior of the robot in the actual working environment and test the steering function of the robot. The magnetic wheel system was able to keep the mobile robot attached to the crawling surface. Next the locomotion ability, functions of the console and communication ability of the robot in actual working environment were tested by running the robot on the ship hull by varying the speed, direction.

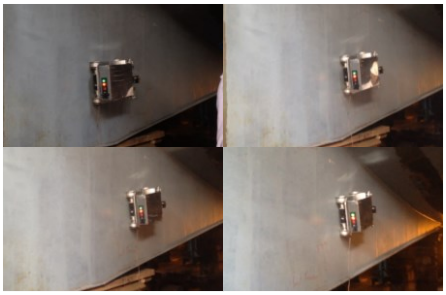

Figure 15. Straight locomotion test

The steering function was tested by navigating the robot on the ship hull surface. The steering system perfectly functioned according to the control inputs provided by the console.

Figure 16. Steering test

The final testing was performed to test the overall performance of the robot. The robot was navigated along a welding seam on the ship hull and inspected it through the camera feed. The testing was done on a ship hull area under the ship and the robot was operated in overhanging orientation.

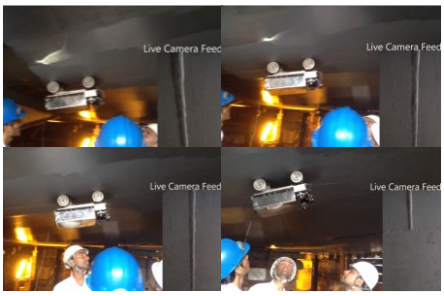

Figure 17. Final test

XI. CONCLUSION

This crawling robot was designed and developed with novel magnetic wheels based on Halbach array. The adhesion force values according to the simulation results could be achieved with the manufactured magnetic wheels. The test results in the similar environment to a ship hull confirmed the ability of the robot to successfully crawl on the ferromagnetic surface and the test results of the robot on the actual ship hull surface ensured the successful function of all the systems of the robot including steering system and camera feedback system.

The main limitations of the robot system are,

1. When the thickness of the crawling surface is decreased the load bearing capacity is diminished.
2. The minimum turning radius of 640.8mm may not be sufficient for the operations in tight areas.
3. The robot needs the human involvement to a certain level in situations such as switching from a surface to another steeply inclined surface.

The performance of the mobile robot can be further enhanced by introducing a suspension system to the robot and accommodating the camber angle to the wheel system. Maximum adhesion forces can be maintained and the robot can crawl on complex and curvier surfaces with the assistance of a suspension system. This crawling robot can be used for other applications such as inspecting the wind turbine towers, tanks and other ferromagnetic structures which are difficult to be reached by an inspector.

REFERENCES

[1] L. Geissmann, M. Denuder, D. Keusch, L. Pfirter, M. Ritter, P. Thoma, R. Siegwart, W. Fischer, G. Caprari, J. Weber, P. Beardsley, Paraswift—"A hybrid climbing and base jumping robot for entertainment", in: Proceedings of the *14th International Conference on Climbing and Walking Robots, CLAWAR, Paris, France, (2011)*, pp. 393–400

[2] C.O. Gil, "Remote-controlled tower maintenance", in: *Wind Systems Magazine (2010)*, pp. 52–55.

[3] M. Spenko, G. Haynes, J. Saunders, M. Cutkosky, A. Rizzi, D. Koditschek, "Biologically inspired climbing with a hexapedal robot", *Journal of Field Robotics 25 (4–5) (2008),* pp. 223–242.

[4] S. Kim, A.T. Asbeck, M.R. Cutkosky, W.R. Provancher, Spinybot II: "climbing hard walls with compliant microspines", in: Proceedings of the *12th International Conference on Advanced Robotics, ICAR, Sousse, Tunesia, (2005)*, pp. 601–606.

[5] Silva, Manuel F., Ramiro S. Barbosa, and António L. C. Oliveira. "Climbing Robot For Ferromagnetic Surfaces With Dynamic Adjustment Of The Adhesion System". *Journal of Robotics* 2012 (2012): 1-16. Web. 19 Jan. 2017.

[6] Tache, Fabien et al. "Adapted Magnetic Wheel Unit For Compact Robots Inspecting Complex Shaped Pipe Structures". *2007 IEEE/ASME international conference on advanced intelligent mechatronics* (2007): n. pag. Web. 19 Jan. 2017.

[7] Zhang, Yuanming et al. "Design And Optimization Of Magnetic Wheel For Wall And Ceiling Climbing Robot". *2010 IEEE International Conference on Mechatronics and Automation* (2010): pp.1393-1398. Aug. 2010

[8] Aaron Burmeister, Narek Pezeshkian, Kurt Talke, Saam Ostovari, H.R. Everett, Abraham Hart, Gary Gilbreath, Hoa G. Nguyen. Space and Naval Warfare Systems Center Pacific. "Design of a Multi-Segmented Magnetic Robot for Hull Inspection". NASA Tech Briefs Magazine. 1st April 2014

[9] Houxiang Zhang, Jianwei Zhang, and Guanghua Zong. "Requirements Of Glass Cleaning And Development Of Climbing Robot Systems". *2004 International Conference on Intelligent Mechatronics and Automation, 2004:*pp. 101-105, August 2004.

[10] Houxiang Zhang, et al. "A Novel Approach To Pneumatic Position Servo Control Of A Glass Wall Cleaning Robot". *2004 IEEE/RSJ International Conference on Intelligent Robots and Systems (IROS) (IEEE Cat. No.04CH37566):* pp.467-468. October 2004.

[11] Sitti, M. and R.S. Fearing. "Synthetic Gecko Foot-Hair Micro/Nano-Structures For Future Wall-Climbing Robots". *2003 IEEE International Conference on Robotics and Automation (Cat. No.03CH37422):* pp 3-10. Sept. 2003.

[12] Nishi, A. and H. Miyagi. "Mechanism And Control Of Propeller Type Wall-Climbing Robot". *Proceedings of IEEE/RSJ International Conference on Intelligent Robots and Systems (IROS'94):* pp.189-194. Sept.1994.

[13] Fondahl, Kristin, Eich, Markus, Wollenberg, Johannes, & Kirchner, Frank (2012) A magnetic climbing robot for marine inspection services. In Bertram, Volker (Ed.) *Proceedings of the 11th International Conference on Computer and IT Applications in the Maritime Industries*, Technische Universit"at Hamburg-Harbur, Liege, Belgium, pp. 92-102.